Heliyon 8 (2022) e12419

Contents lists available at ScienceDirect

Heliyon

journal homepage: www.cell.com/heliyon

Research article

Delimiting radiation protection distance of underground uranium mining and metallurgy facilities: A case study in China

Hui Zhang, Jie Gao, Yunlong Bai, Lei Zhou, Lechang Xu *

Beijing Research Institute of Chemical Engineering and Metallurgy, CNNC, Beijing, China

ARTICLE INFO

Keywords:
Uranium mine
Ventilation shaft
Short-term radon concentration
Distribution regularities

ABSTRACT

Delimiting radiation protection distance of uranium mining and metallurgy facilities is an important radiation protection approach to control the effective public dose caused by radon and radon progeny. Ventilation shafts are the main radon release paths of underground uranium mines. It is of great importance to research the diffusion regularities and influence range of the radon around the ventilation shaft. In this study, long-term and short-term radon accumulation monitoring approaches were adapted for onsite investigation. More than 520 sets of radon concentration were acquired. The survey results effectively revealed the distribution regularities of the radon concentration around the ventilation shaft with time, space, and working conditions. These results provide data for radiation protection in uranium mines. In addition, a radiation protection distance delimiting way was proposed for the investigated facility through effective public dose assessment.

1. Introduction

As the foundation of nuclear energy, uranium mining and metallurgy (UMM) is facing new developing opportunities as well as challenges from stricter radiation safety management. Over 85% of internal exposure hazard and 76.7% of the collective effective dose are caused by radon and radon progeny of UMM(Zhou et al., 2019). And for a underground UMM, 95% of radon is discharged by the ventilation shaft. A comprehensive understanding of the radon concentration distributions around ventilation shafts of underground uranium mines is of great importance for radiation protection in underground uranium mining and metallurgy. Usually, the radiation protection regulatory measures are carried out based on radiation environmental impact assessment suggestions and relevant radiation dose estimation results, which are based on the concentration of radon and radon progeny diffusion into the ambient air (Vandenhove et al., 2006). Therefore, effective investigation and determination of the diffusion and distribution of radon and radon progeny are a prerequisite for the in-depth development of radiation protection measures in uranium mines, such as setting the radiation protection distance, relocation of the surrounding residents (Unger et al., 2020), and radiation protection project implementation (Gaskin et al., 2019). In China, formerly, a unified and more conservative radiation protection distance was adapted by the regulators which brought the operators heavy burden on land acquisition and environmental investment.

Environmental radon concentrations and distributions around UMM facilities are usually acquired through onsite monitoring and model estimation (Kovalets et al., 2017). Model simulation is the most convenient method of acquiring the radon distribution, but the accuracy of this method is barely satisfactory. Onsite monitoring can provide accurate first-hand data, but it is impossible to obtain hundreds of qualified onsite data at the same time in all directions.

The Y30AIR model and the American Meteorological Society/Environmental Protection Agency regulatory model (AERMOD) are the most commonly used atmospheric diffusion models for uranium mines in China (Ma et al., 2013). The Y30AIR model is a radioactive gas pollutant concentration prediction software that has been widely used in UMM. The AERMOD is recommended by the Ministry of Ecology and Environmental of the People's Republic China, and it has been widely used for non-radioactive environmental impact assessment and has recently been used in UMM. In addition, numerous air pollution diffusion models, including the California puff (Cal-puff) model (Han and Kim, 2021) and the atmospheric dispersion modeling system (ADMS) model (Dong et al., 2021), are commonly used for environmental impact assessment of other types of nuclear facilities. Although most demanding concentration prediction and dose estimation calculations are solved using the above mentioned models, to some extent, there are still defects. For example, it is difficult to process the radioactive decay chain using AERMOD. There are some problems in dealing with meteorological issues such as a local

* Corresponding author.
E-mail address: lechangxu_bricem@126.com (L. Xu).

https://doi.org/10.1016/j.heliyon.2022.e12419
Received 11 September 2022; Received in revised form 1 November 2022; Accepted 9 December 2022

reverse temperature layer and the atmospheric stability boundary layer in the Y30AIR model. Therefore, when radiation supervision measures need to be designed, obtaining the estimation model using only the radon and radon progeny distributions is far from sufficient.

Onsite monitoring is an effective way of researching the radon distribution, but there are difficulties in the representativeness. The monitoring plan should be improved to summarize the spatial and temporal radon distributions. Durridge RAD7 (Durridge, 2011) is used for instantaneous radon detection during short sampling periods, and the radon concentration level is only characterized under specific conditions, which does not reflect the systemic radon concentration level of the entire area. It is feasible to increase the measurement time of radon concentration detection for one point, but it is impossible to simultaneously sample hundreds of points since their individual concentrations would change with time. Passive radon detection methods such as the activated carbon box satisfy the need for simultaneous sampling but are limited by the humidity of the site. The humidity of the ventilation shaft of UMM is >98%, which is too high for use of an activated carbon box (Zhou et al., 2019).

In this study, the distribution of the radon concentration around an underground UMM ventilation shaft in different directions and at different distances within a 1-km radius was fully studied and compared with the atmospheric model estimation results. The radon diffusion and distribution regularities were analyzed through case studies, and the effective public dose caused by the release of radon from the ventilation shaft was evaluated. Finally, policy recommendations about the radiation protection distance of UMM facilities were developed.

2. Methods and instruments

2.1. Methods

In order to meet the investigation requirements of simultaneous multi-point measurement of the distribution regularities and to improve the data quality, the field investigation in this study included both long-term and short-term cumulative radon detection approaches. Durridge RAD7 is also used for instantaneous radon monitoring.

The interference factors should be considered when selecting the method, including the measurement position, principle of the measuring instrument, equipment model, equipment background level, skill of the operators, surrounding facilities, temperature, pressure, humidity, sun irradiation, measuring time, season, wind direction, wind speed, and air pressure (Yarmoshenko et al., 2021). Measures that can be used to improve the representativeness of the radon concentration monitoring data include improving the accuracy of the equipment, reducing the instrument's background level, excluding external interference factors, and increasing the sampling coverage of the measurements (Davies and Britton, 2020; Elísio and Peralta, 2020).

Long-term cumulative radon detection approach usually refers to the cumulative detection approach with a sampling time interval longer than several times the half-life of radon, i.e., several weeks or months. Short-term cumulative radon detection approach usually refers to the short-term cumulative detection approach with a cumulative detection time, which is longer than 1 day and does not exceed the half-life of radon (3.85 days) (Fijałkowska-Lichwa, 2014). In this study, the solid state nuclear track detector (SSNTD) (Girault and Perrier, 2012) method was selected as the environmental long-term cumulative radon concentration detection approach, and the positive electric electret radon measurement was selected as the short-term cumulative radon detection approach. The KF-606B (Liu et al., 2017; Zhou et al., 2019) solid nuclear track cumulative radon detector produced by the Beijing Institute of Chemical Industry and Metallurgy, China, was selected as the long-term cumulative radon concentration detection instrument, and the E-perm electret (Kotrappa et al., 2013; Shweikani et al., 2014) radon detector produced by Red Elec, USA, was selected as the short-term cumulative radon concentration detection instrument.

2.2. Instruments

A schematic diagram of the KF606B is shown in Figure 1. The device is made from acrylonitrile butadiene styrene (ABS) engineering resin. There is a maze gas inlet in the lower part of the dosimeter. The sample air is filtered through the filter membrane and enters the diffusion chamber. The designed diffusion time is 15 min from the inlet to the detector, which effectively responds to the radon and prevents 95% thoron. The detection sensitive element CR-39 is placed at the center of the bottom of the diffusion chamber. The α particles from radon and radon progeny decay hit the CR-39 detector to form latent tracks. The environmental radon concentration is measured using the linear relationship between the track density per unit area and radon concentration during the accumulation time.

The E-Perm electret radon measuring device is suitable for a variety of environment measurements. The instrument consists of three parts: a positive electret, an ionizing chamber, and an electrostatic potential meter. The short-term cumulative radon and long-term environmental cumulative radon can be monitored using different ionizing chamber combinations. The measurement system has low limits for the environment and can be measured under humidity and temperature conditions of RH% < 100% and T < 50 °C. The principle of the instrument is shown in Figure 2.

3. Onsite monitoring

3.1. Onsite investigation plan

In order to effectively investigate the distribution regularities of the radon concentration within 1000 m of the underground UMM ventilation shaft, multi-directional ray distribution was used in this study. Sixteen directions and eight points for each direction were set as the monitoring points for the short-term radon monitoring. The 16 directions were N, NNE, NE, ENE, E, ESE, SE, SSE, S, SWS, SW, WSW, W, WNW, NW, and NNW; and the eight distances were 50 m, 100 m, 200 m, 300 m, 400 m, 500 m, 800 m, and 1000 m. All of the points needed to be monitored at nearly the same time.

Six directions around and eight points in each direction were set as the monitoring points for the long-term radon monitoring. The six directions included three pairs of wind directions, the directions the winds came from, and the directions the winds blew toward. The dominant wind frequency direction pair (WSW and ENE), the minimum wind frequency direction pair (upwind SE and downwind NW), and the middle wind frequency direction pair according to the field situation (N and S) were selected.

The long-term and short-term cumulative radon monitoring methods were used, and instantaneous continuous radon monitoring was used as support.

The monitoring investigation lasted for 1 year. The short-term cumulative radon detection period was 8–48 h at each point, and one batch was collected during the production period and another was collected during the shutdown period. The long-term cumulative radon detection cycle was 90 days for each batch, and there were four batches in total, i.e., two under production conditions and two under shutdown conditions. The instantaneous radon continuous monitoring included 72 h of continuous monitoring under the working conditions.

3.2. Meteorological conditions

An underground uranium mine in southern China was chosen as the investigation objective. The site had a mild and humid monsoon subtropical climate, with abundant rainfall and a mountain climate. The regional relative humidity was 55%–94%, the annual average temperature was 17.4°C–21.2 °C, the annual average sunshine was 1690 h, the minimum temperature was −6 °C, and the highest temperature was 36.9 °C. The annual average rainfall was 1573.3 mm, and the average

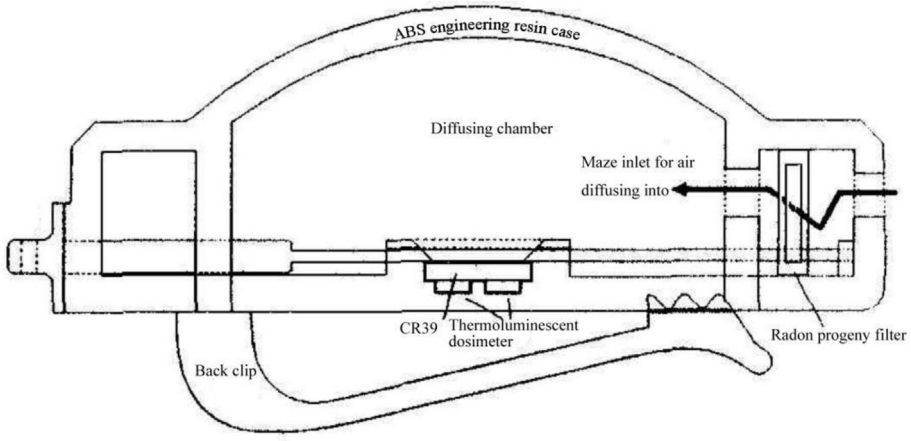

Figure 1. Schematic diagram of the KF606B.

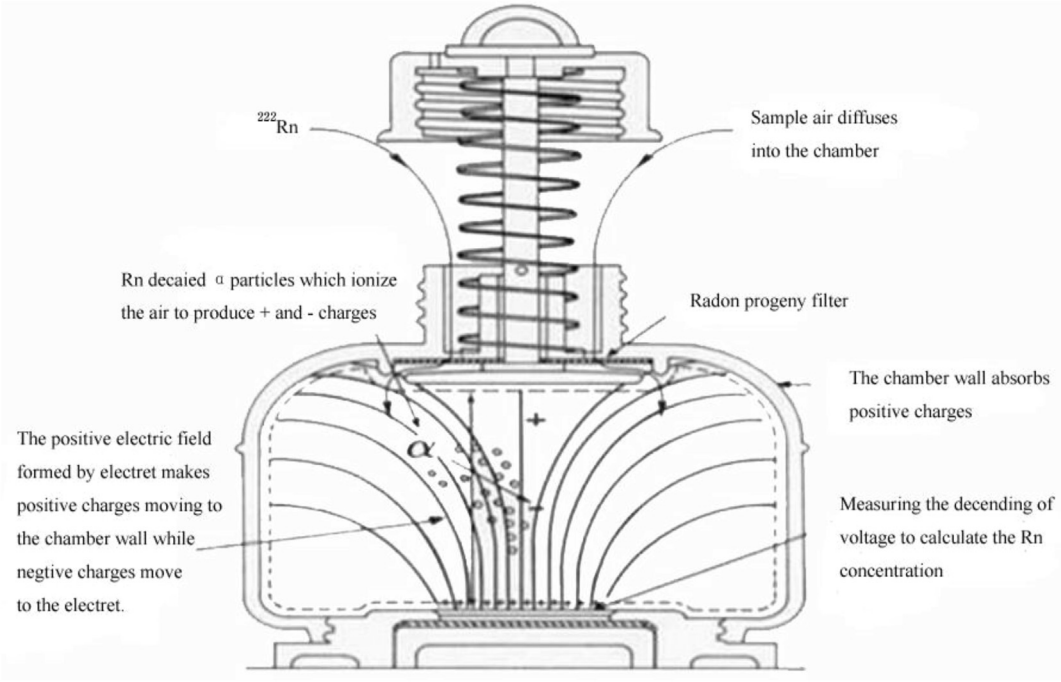

Figure 2. Schematic diagram showing the principle of electret radon measurement (Shweikani et al., 2014).

evaporation was 1497.1 mm. Precipitation was rare in autumn and winter, and the rainy seasons were concentrated in February and July. The annual dominant wind direction of the site was ENE, the wind frequency exceeded 42%, the annual average wind speed was 1.5 m/s, and the annual average air pressure was 9.98×10^4 Pa.

3.3. Overview of ventilation shaft and surrounding environment

The ventilation shaft was circular, with an internal diameter of 3.5 m, an external height of 2.5 m above the ground, a wall thickness of 30 cm, and a vertical section depth of 380 m. There was a safety grille located at a distance of 2.5 m inside the pipe. The ventilation volume of the shaft was about 60 m^3/s, and the mean radon concentration was 37.5 kBq/m^3 (Zhou et al., 2019). The ventilation shaft was located in a dense plant covered mountainous area. The ventilation shaft was located at the intersection of two valleys. The altitude was 140–260 m within the study area. Overall, the altitude in this terrain was high in the southwest and slightly lower than in the northeast. There were no obvious radon release sources within 1.8 km of the ventilation shaft which can be seen from Figure 3, thus, the contribution and influence of other radon release sources on the radon concentration within the study area were ignored. There were no UMM facilities or tailing piles or waste rock piles around the ventilation shaft within 1.8 km. According to an investigation held at the same time of this research, the radiation environment of the research area was the same level of regional background level. The ambient gamma radiation dose rate was 102 to 137 nGy/h, the surrounding soil radioactivity of nature uranium and ^{226}Ra are 58.1 Bq/kg and 32.5 Bq/kg.

3.4. Monitoring organization and implementation

The monitoring began in early June of the first year and continued until the end of the second year. From June of the first year to May of the second year, the long-term cumulative radon monitoring was carried out using a KF606B in six directions around and eight distances from the ventilation shaft. From June of the first year to November of the first

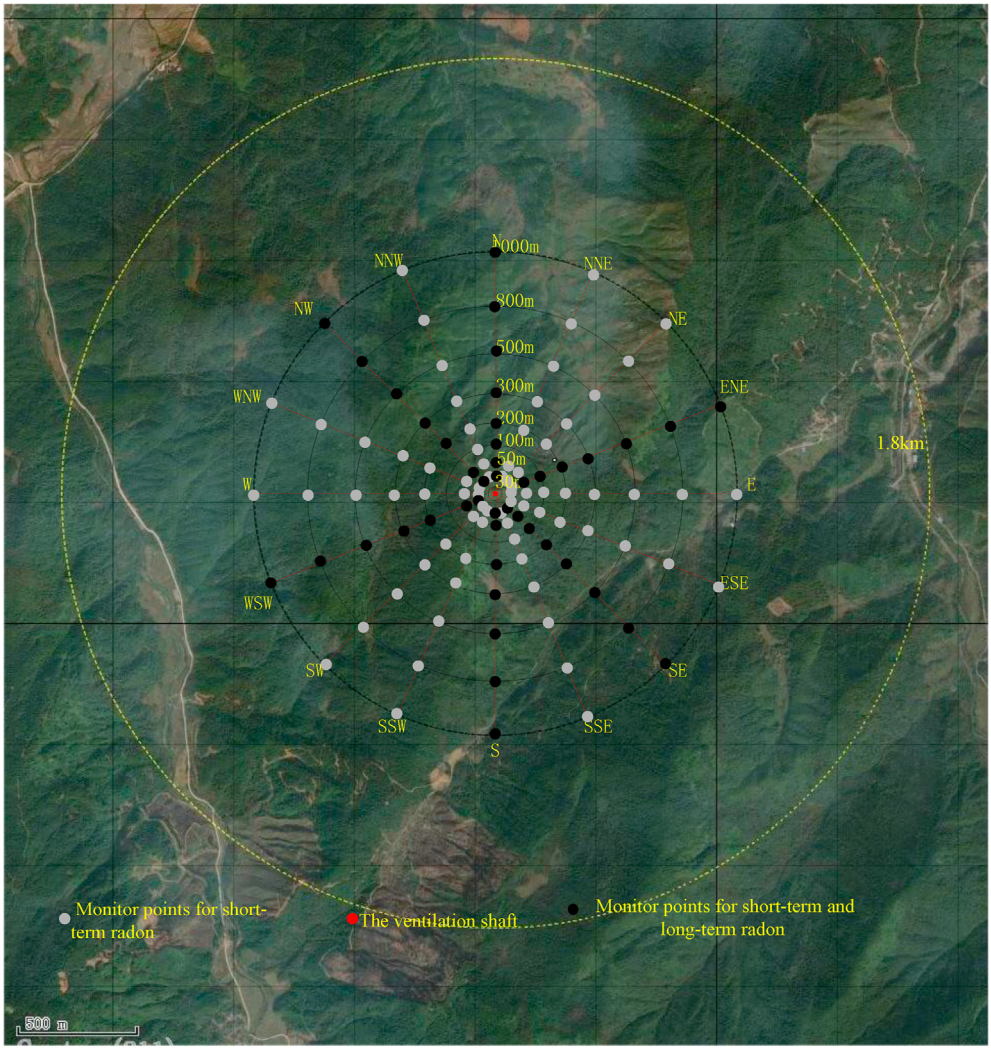

Figure 3. Diagram of topography around the ventilation shaft and the monitoring points.

year, two batches of radon concentration data were monitored around the ventilation shaft under production conditions. From December of the first year to May of the second year, the other two batches were measured during shutdown. Three blank samples were collected with each batch by closing the gas inlet switch to provide a background reference.

The short-term cumulative radon monitoring was conducted in September of the first year and February of the second year in 16 directions around and eight distances from the ventilation shaft. During the production period, after several continuous fine days the monitoring were carried out. The monitoring data for September of the first year represented the production conditions, and the monitoring data for February of the second year represented the shutdown conditions.

The instantaneous continuous radon sampling and monitoring were treated as auxiliary radon monitoring means. RAD7 radon monitoring was carried out at the point about 500 m to the WSW under normal production conditions in September of the first year. It is used for continues radon monitoring.

Radon detectors are generally placed in a barrier free space ranging from 1 m to 1.5 m above the ground. The long-term cumulative radon and short-term cumulative radon sample layout adopted simultaneous sampling, that is, the time between the first and last samples of the long-term cumulative radon batch monitoring was no more than 24 h, while that of the short-term cumulative radon monitoring was no more than 3 h to ensure the temporal consistency of the data. The distribution process randomly increases to 10% parallel samples in order to verify the quality of the monitoring data.

4. Monitoring results

The long-term cumulative radon concentration monitoring data for six directions around and within 1000 m of the ventilation shaft are presented in Table 1 There were at least 192 long-term cumulative radon concentration data. It can be seen from the table that the maximum radon concentrations in the different directions were not in the positions closest to the ventilation shaft and were generally located 100–200 m from the shaft. The concentration gradually decreased beyond 300 m. The impact of the radon concentration at 500 m was significantly reduced, and it was the same as the local background level at 800 m. Compared with the normal production and shutdown periods, the radon concentration decreased significantly, except for the 500-m point in the ENE direction. The maximum radon concentration (1732.1 Bq/m^3) was measured at 100 m in the WSW direction, and the relative radon concentration at this point decreased to 68.5 Bq/m^3 or 65.7 Bq/m^3 under the shutdown conditions.

Totally 256 effective short-term cumulative radon figures were acquired. The figures range from 28.2 ± 3.6 Bq/m^3 to 1532.6 ± 143.2 Bq/m^3. The short-term cumulative radon data were processed using the kriging interpolation method in order to draw a distribution contour map (Loffredo et al., 2021). Figure 4 shows the contour map of the radon concentration within 1000 m of the ventilation shaft under production conditions, and Figure 5 shows the contour map of the radon concentration under shutdown conditions. It can be seen from the figures that the quantity of radon released from the shaft contributed

Table 1. Long-term cumulative radon monitoring results (Bq/m^3).

Directions	Work condition	Distance from the center of the ventilation shaft			
		50m	**100m**	**200m**	**300m**
N	Producing	222.9 ± 6.7	183.3 ± 16.5	621.5 ± 55.9	170.7 ± 11.9
	Producing	235.2 ± 21.2	176.3 ± 14.1	700.2 ± 21.	190.2 ± 11.4
	shutdown	38.7 ± 1.2	70.2 ± 8.4	67.5 ± 6.1	57.4 ± 4.6
	shutdown	40.5 ± 2.	75.4 ± 8.3	62.5 ± 3.1	62.1 ± 5.6
ENE	Producing	279.5 ± 22.4	150.4 ± 4.5	615.3 ± 24.6	189.1 ± 18.9
	Producing	293.4 ± 32.3	170.5 ± 6.8	690.4 ± 55.2	161.4 ± 9.7
	shutdown	72.5 ± 4.4	70.5 ± 2.1	63.4 ± 4.4	72.5 ± 7.3
	shutdown	69.4 ± 2.8	72.1 ± 5.	65.4 ± 3.9	72.9 ± 2.9
SE	Producing	293.2 ± 20.5	148.1 ± 17.8	492.7 ± 34.5	111.3 ± 8.9
	Producing	259.5 ± 28.5	157.3 ± 12.6	505.6 ± 50.6	120.5 ± 14.5
	shutdown	38.5 ± 3.9	38.5 ± 3.5	42.6 ± 1.7	55.4 ± 3.9
	shutdown	45.2 ± 2.3	39.5 ± 3.2	48.5 ± 4.4	52.4 ± 5.2
S	Producing	540.2 ± 37.8	688.7 ± 82.6	1065.1 ± 117.2	149.9 ± 10.5
	Producing	588.5 ± 29.4	439.7 ± 13.2	1299.5 ± 39.	179.4 ± 12.6
	shutdown	62.2 ± 7.5	56.4 ± 3.9	49.1 ± 2.	36.5 ± 2.2
	shutdown	61.5 ± 1.8	63.5 ± 4.4	46.7 ± 2.8	42.3 ± 1.7
WSW	Producing	262.9 ± 28.9	**1732.1 ± 103.9**	1482.8 ± 59.3	162.7 ± 8.1
	Producing	266.3 ± 16.	**1654.5 ± 165.5**	1640.4 ± 114.8	179.5 ± 10.8
	shutdown	67.2 ± 3.4	68.5 ± 6.2	57.6 ± 2.9	40.2 ± 4.4
	shutdown	68.4 ± 4.1	65.7 ± 7.9	64.3 ± 3.9	44.3 ± 4.9
NW	Producing	262.1 ± 28.8	216.5 ± 13.	899.4 ± 27.	253.3 ± 22.8
	Producing	304.5 ± 12.2	279.2 ± 30.7	917.3 ± 73.4	221.5 ± 24.4
	shutdown	66.2 ± 5.3	72.3 ± 3.6	68.1 ± 4.1	42.5 ± 5.1
	shutdown	69.1 ± 6.9	78.4 ± 7.8	62.4 ± 3.1	48.6 ± 5.8
		400m	**500m**	**800m**	**1000m**
N	Producing	125.4 ± 7.5	69.4 ± 4.9	41.5 ± 3.3	42.3 ± 2.5
	Producing	132.1 ± 13.2	71.6 ± 2.1	42.1 ± 1.7	39.5 ± 3.2
	shutdown	58.9 ± 2.9	52.6 ± 3.2	37.4 ± 4.1	28.6 ± 2.3
	shutdown	64.5 ± 6.5	41.5 ± 1.2	43.2 ± 1.3	30.5 ± 3.1
ENE	Producing	125.9 ± 3.8	66.9 ± 3.3	49.3 ± 2.	36.3 ± 4.4
	Producing	154.8 ± 13.9	62.3 ± 3.1	48.6 ± 1.9	49.3 ± 2.5
	shutdown	123.4 ± 14.8	**237.3 ± 19.**	43.5 ± 3.9	32.4 ± 1.
	shutdown	109.5 ± 3.3	**242.4 ± 21.8**	44.6 ± 3.6	35.6 ± 3.2
SE	Producing	86.2 ± 5.2	56.2 ± 2.8	43.3 ± 4.3	38.2 ± 3.4
	Producing	75.2 ± 3.	55.6 ± 5.	39.4 ± 3.5	40.1 ± 3.6
	shutdown	50.3 ± 2.5	46.5 ± 3.7	36.4 ± 4.	34.7 ± 2.4
	shutdown	42.4 ± 3.	45.5 ± 2.7	30.5 ± 3.7	35.4 ± 1.1
S	Producing	94.3 ± 3.8	42.7 ± 5.1	39.8 ± 2.8	32.5 ± 2.3
	Producing	102.5 ± 4.1	48.5 ± 1.9	45.5 ± 5.5	42.1 ± 2.9
	shutdown	70.2 ± 7.7	42.5 ± 1.7	40.5 ± 1.6	28.5 ± 3.4
	shutdown	68.5 ± 5.5	39.4 ± 2.	34.2 ± 1.4	36.2 ± 1.4
WSW	Producing	98.9 ± 7.9	48.1 ± 2.9	42.3 ± 1.3	38.8 ± 1.6
	Producing	101.5 ± 11.2	43.6 ± 5.2	42.5 ± 3.8	37.6 ± 4.1
	shutdown	46.5 ± 1.4	43.5 ± 4.4	35.4 ± 4.2	36.9 ± 3.7
	shutdown	35.5 ± 2.8	45.4 ± 3.2	38.5 ± 3.5	34.9 ± 2.4
NW	Producing	146.3 ± 8.8	50.2 ± 2.5	50.3 ± 3.5	37.6 ± 2.3
	Producing	130.2 ± 11.7	52.3 ± 5.8	44.2 ± 4.	32.6 ± 3.3
	shutdown	44.9 ± 4.9	37.9 ± 3.4	41.8 ± 2.5	39.4 ± 2.
	shutdown	39.5 ± 3.6	41.2 ± 4.1	36.5 ± 4.	40.3 ± 4.4

Direction means take the shaft as center where the monitoring site is to directinos as north, south etc. Work condition refers to the working condition of mining and metallurgy facilitities when the monitoring took place, there are two work condition, producing and shut down. Distance from the center of the ventilation shaft refers the distance form the shaft center to the monitoring sites. and the relevent monitoring value lists in the table.

significantly to the levels in the surrounding environment. Part of the concentration distribution was mainly affected by the meteorological conditions, such as the wind speed and wind direction. An area of high radon concentration was formed in the WSW direction at about 100–200 m from the shaft, and the radon concentration rapidly decreased and reached the background level at 400–500 m from the shaft. The radon concentration decreased slower in the ENE direction than in the WSW direction.

As can be seen from Figure 5, the environment radon concentration rapidly decreased to the background level after production stopped, except for the ENE direction. There was an area where the radon concentration was higher than 100 Bq/m^3. It was later confirmed that radon was escaping from an unblocked emergency escape shaft that had been abandoned a long time ago.

In order to compare the data, a contour map was also drawn using simulation data. The distribution of the radon concentration within 1000 m of the ventilation shaft was estimated using the AERMOD. Figure 6 shows the radon concentration distribution regularities analyzed using the simulation data for production conditions. The simulation data only consider the radon contribution; in order to compare the simulation data with the onsite monitoring data, 28 Bq/m^3 was selected as the regional background radon concentration. It can be seen that the simulation underestimates the radon contribution to the nearby environmental radon concentration, and the estimation of the radon migration and diffusion and distribution regularities is quite different from the field detection results.

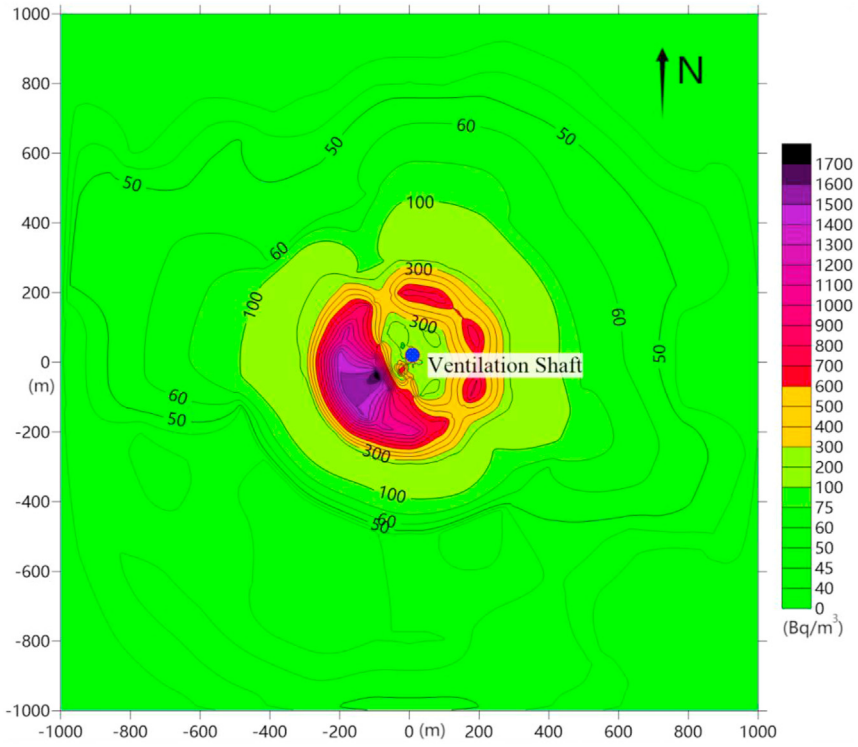

Figure 4. Contour diagram of the monitored radon concentrations around the ventilation shaft under production conditions.

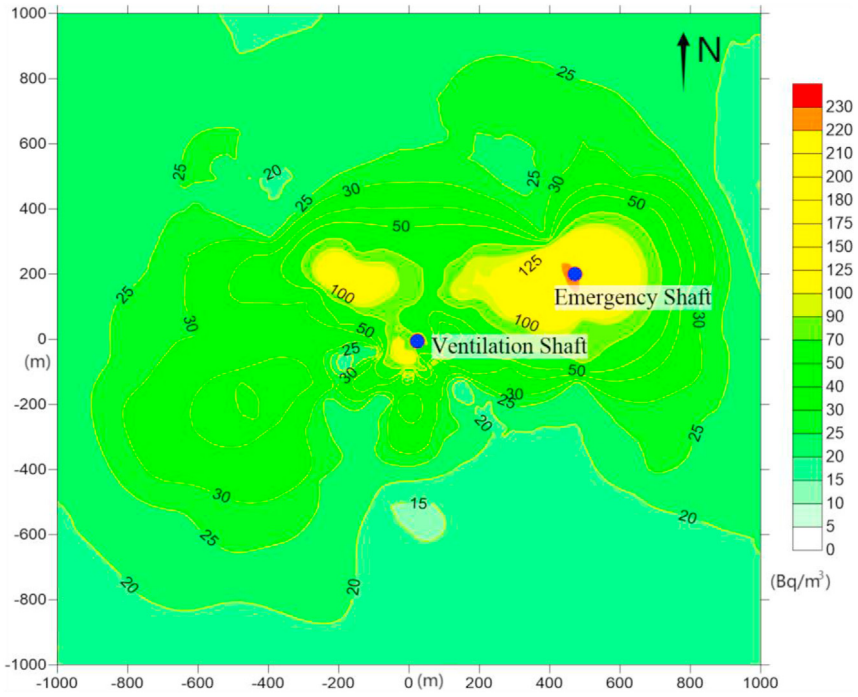

Figure 5. Contour diagram of the monitored radon concentrations around the ventilation shaft under shutdown conditions.

5. Discussion

5.1. Basic distribution regularities around the ventilation shaft with distance

Table 1 presents the long-term cumulative radon concentration in the six directions. The ventilation shaft was a typical underground UMM radon release structure, and its surrounding ground radon concentration was initially low and then high. Then, it gradually decreased to the background level. The obvious radon impact distance was generally less than 800 m.

The radon diffusion from a centralized source is influenced greatly by the wind speed and wind direction. By comparing the shutdown and production data, it can be seen that except for the unexpected emergency

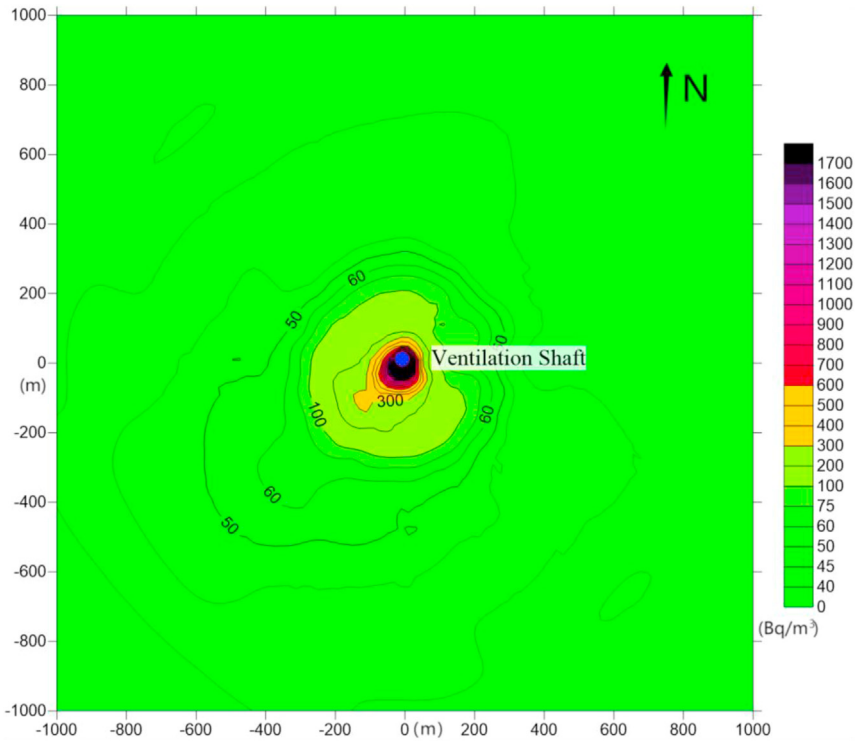

Figure 6. Contour diagram of the simulated radon concentration data around the ventilation shaft.

shaft area, the radon concentrations decreased significantly in the different directions, and it decreased more in the area closer to the shaft. The average radon reduction in the different directions was greater than 139.5 Bq/m^3, the most significant decrease occurred in the WSW direction, and the average radon reduction reached 439.9 Bq/m^3. For the different directions, the areas downwind of the dominant wind direction were greatly affected by the shaft, and the maximum ground radon concentration was measured 100 m from the shaft in the WSW direction. The radon concentration decreased rapidly and reached the background level more quickly in the WSW direction than in the ENE direction, that is, the radon diffused more quickly in the downwind direction than in the upwind direction. The reason for this is that the pollutant (i.e., the radon) that diffuses in the upwind direction is blown back by the wind and overlaps with the new diffusing radon, making the radon diffuse more slowly in this direction. This can also be seen from Figure 4, in which the contours are far denser in the WSW direction than in the ENE direction.

In addition to being affected by wind speed and wind direction, the diffusion of the radon concentration is also an important factor. Figure 4 shows that a fan-shaped high-concentration area formed to the WSW of the ventilation shaft due to the wind speed and wind direction. The radon concentration in the downwind area of the dominant wind direction rapidly decreased to the background level. Although the radon decreased with distance in the NE, ESE, and WNW directions, the radon concentration in the ENE direction decreased more slowly than in the WSW direction. In addition to the radon superposition problem in the ENE direction (i.e., the radon diffuses in the ENE direction and is blown back and admixed with the new diffused radon), the fan-shaped high radon concentration area in the WSW direction acts as a high radon concentration wall that the radon from the ENE direction cannot climb over. This is another reason why the radon concentration decreased more slowly with distance in the ENE direction than in the WSW direction.

5.2. Daily radon distribution regularities and monitoring influences

Focusing on different distances and different radon concentration changes with time in the ENE and WSW directions (upwind and downwind of the maximum wind frequency), radon concentration monitoring using different methods in different periods was adopted for these two directions. The characteristics of the changes in the radon concentration in the ENE and WSW directions are shown in Figure 7. A comparison of the long-term and short-term results for these two directions is shown in Figure 8. DAY refers to the monitoring data collected during the daytime (7–9 a.m. to 6–8 p.m.). NIGHT refers to the monitoring data collected at night (7–9 p.m. to 8–10 a.m.). 24 H refers to the short-term accumulation monitoring data collected during a 24-h sampling period using electret. KF refers to the long-term accumulated radon data collected using the KF606B during a 90-day period.

As shown in Figure 7, the radon concentrations decrease with distance in the two directions. Because WSW is the dominant wind direction, the radon concentration is significantly higher than in the upwind direction, and the maximum value was measured at 100 m, while the maximum value in the ENE direction was measured at 200 m, and it was only about 1/3 of the maximum value in the WSW direction. The data obtained during the different periods and using different detection methods are significantly different. However, in both directions, the radon concentration decreased to the background level within 500 m.

Some useful information can be obtained from the data collected using different monitoring methods and during different sampling periods. Figures 7 and 8 show the radon concentration distribution in the ENE and WSW directions. It can be seen that the NIGHT monitoring data are generally higher than the DAY data at the same distance. For example, in the ENE direction at 100 m and 200 m, and in the WSW direction at 100 m, 200 m, and 500 m, the NIGHT concentrations are 2 times higher than the DAY concentrations, and the concentrations at the other points at night are at least 50% higher than the corresponding concentrations during the day. Based on the long-term radon concentration data, the NIGHT data are generally 20% to 50% higher than the KF data. It can be concluded that for fine weather, the radon concentration in the open environment near the ventilation shaft is higher at night than during the day.

In order to verify the diurnal radon concentration changes, after several consecutive days of fine weather, 72-h continuous radon

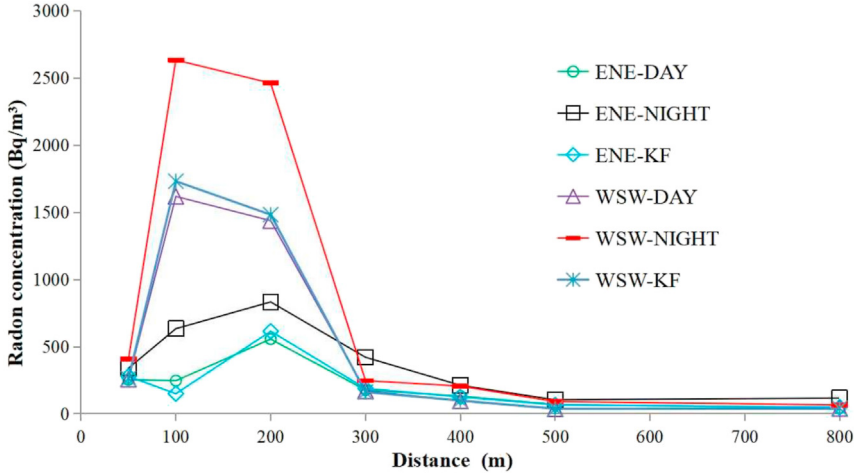

Figure 7. Radon concentrations in the ENE and WSW directions at different distances and monitoring times.

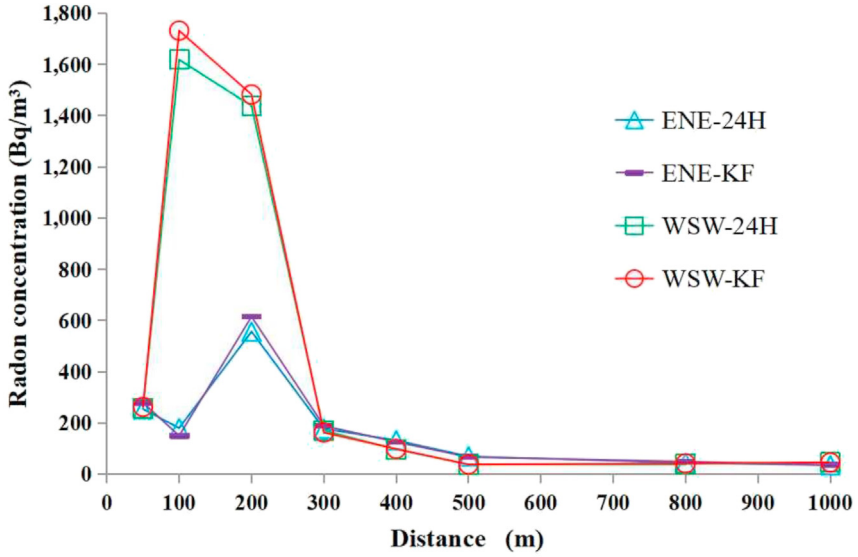

Figure 8. Comparison of the long-term and short-term monitoring data in the ENE and WSW directions.

observations were carried out at the 500 m point in the WSW direction from 14:12 on the first day to the same time on the fourth day using a Durridge RAD7. The results are shown in Figure 9.

The continuous radon monitoring results show that the radon concentration in the open environment is higher at night than during the daytime. The radon concentrations gradually decrease from around 07:00 to 09:00 and increase from 18:00 to 20:00. The overall radon concentration is lower during the day than at night, and the maximum concentration difference at the same point reaches 60 Bq/m^3. It was assumed that different thermal behaviour between air and soil make the radon exhale from soil slower in the daytime than in night. In this research, most of the ground covered with plant and it could not be illuminated directly by the sun. In the day time, the ground temperature ascended mostly by heat conducted from the surround air. The soil was colder and exhaled less radon while the heater air made radon easy diffusing. while in the night the situation was to the contrary. This theory need be verified in subsequent studies.

The results of the radon concentration monitoring during the different periods are different, and the radon concentration at a given point is significantly higher at night than during the day. As can be

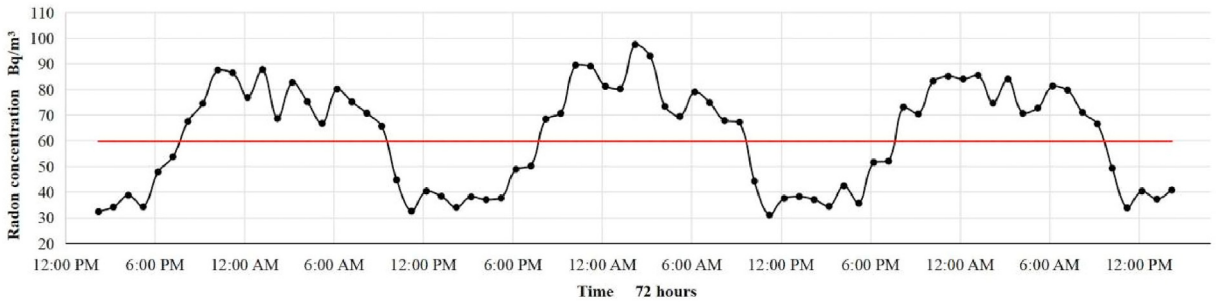

Figure 9. Results of the 72-hours continuous radon monitoring.

concluded from Figure 8, the 24-h short-term cumulative radon results are highly consistent with the 90-day long-term cumulative radon monitoring results. These two data series at two different locations are highly correlated (Figure 8). The reason for this is that the short-term cumulative radon monitoring effectively covers the main period of radon concentration change, and its average value is similar to the average effect of the long-term cumulative radon. Considering the inconvenience of acquiring long-term monitoring data, it is possible to use short-term 24-h accumulation radon monitoring data instead of long-term accumulation radon monitoring data. However, the meteorological and diffusion conditions should be appropriately considered. In practice, 24-h short-term accumulation radon is representative and can be obtained more easily. However, not all of the 24-h radon concentration data are appropriate, and 24-h cumulative monitoring should be carried out under continuous fine weather conditions.

5.3. Comparison of the radon distribution contour maps

The distribution regularities of the regional radon concentration can be effectively determined through monitoring and interpolation analysis.

By comparing Figures 4 and 5, it can be seen that the radon concentration around the UMM shaft decreased rapidly after shutdown of the ventilation shaft and most of the areas decreased to the background level, except for the abnormally high radon concentration area in the ENE direction where an abandon emergency shaft was later observed. During production, the ventilation fan causes the abandoned shaft to serve as an air inlet. After shutdown, the ventilation was shut off, and the high concentration radon gas dispersed through the emergency shaft, which led to the high concentration area in Figure 6. The fact that this unexpected emergency shaft was identified using the contour map proves that field radon concentration investigation and interpolation analysis can effectively reveal the distribution characteristics of the radon concentration.

There is a huge difference between the atmospheric mode estimation data and the monitoring data. Comparison of Figures 4 and 6 reveals that there are differences between the numerical simulation and distribution pattern. First, the radon concentration contribution of the simulated data is generally lower than that of the field detection data. Although the estimated data may be affected by the selection of the background value, the contour map still cannot effectively express the distribution characteristics of the radon concentration around the ventilation shaft, especially the radon diffusion regularities in the ENE and WSW directions. The simulated radon concentration within 50 m of the ventilation shaft is 467–3942 Bq/m^3, which is higher than the actual concentrations.

In the SSW, SW, WSW, and W directions, the predicted values are 2722–3942 Bq/m^3 higher than the measured values. The simulated radon concentrations at distances of 200–300 m are 20–200 Bq/m^3 higher than the monitoring results, while the simulated radon concentrations at distances of 300–800 m are approximately 3–20 Bq/m^3 lower than the monitoring results.

In the ENE direction, the estimated radon concentrations are 10–500 Bq/m^3 lower within 300 m, while they are generally 10–33 Bq/m^3 lower at distances of 400–800 m. Beyond 800 m, the AERMOD model predicts that the ventilation shaft contributes 7–17.5 Bq/m^3 to the environment, which is very close to the monitoring results. Therefore, the model estimation results alone cannot accurately reflect the distribution of the radon concentration around the ventilation shaft, and the model results need to be analyzed in combination with other data sources (Xie et al., 2014). In addition, the local diffusion of radon is highly correlated with the topography and type of surface, and the degree and mode of similar influencing factors should be further investigated.

5.4. Policy implications for the radiation protection distance

The radiation protection distance of UMM facilities is an important approach for stakeholders to reduce exposure to radioactive environments in practice (Brusin, 2007). The radon concentration distribution data can help the authorities and operators determine the radiation protection distance. The radiation protection distance is the distance from the boundary of the facilities to the nearest resident. It is a preventative regulation that prevents excessive public doses via spatial protection (De Pree, 2020).

The Regulations on Radiation Protection and Environmental Protection of Uranium Mining and Metallurgy, a national standard for UMM, stipulates that "the facilities shall determine the radiation protection distance from the residential areas through environmental impact assessment according to the nature of the pollution sources, the local natural and meteorological conditions, and other factors, but the minimum distance shall not be less than 300 m" It is insufficient for conventional UMM facilities to only meet the minimum radiation protection distance requirements, and the radiation protection distance should be determined through radiation environmental impact assessment. The standard also stipulates that "the dose constraint of public exposure during the operation period is an average effective dose of 0.5 mSv/a". Therefore, the radiation protection distance should meet the requirements of the distance, and active protection or relocation should be conducted to meet the requirements.

The equation for calculating the effective dose of radon and radon progeny is as follows (Chen, 2005):

$$E_{Rn} = f \times D \times C_{Rn} \times g, \quad (1)$$

where E_{Rn} is the effective public dose caused by inhaling radon and radon progeny (mSv/a); and f is the number of days in 1 year (8.76×10^3 h). D is the residence factor, which is usually 0.2, and the rural residence factor is 0.3, which refers to the proportion of time people stay in the evaluation environment (Obodunrin, 2022). C_{Rn} is the air radon concentration contributed by production activities (Bq/m^3); g is the radon progeny inhalation dose conversion factor (3.66×10^{-6} mSv/(h.Bq/m^3)) recommended by the United Nations Scientific Committee on the Effects of Atomic Radiation (UNSCEAR) (Marsh et al., 2021). Considering the changes in the age structure and living habits of rural residents in China, the scenario in which the residence factor of the people around the facilities reaches 0.4 is discussed. The public effective dose of radon and radon progeny in the gas phase accounts for at least 76.7% of the total effective dose, and the proportion will gradually increase with further optimization of radiation protection measures. Considering that this proportion reaches 80%, that is, the contribution of radon and radon progeny should be less than 80% of 0.5 mSv/a (the effective public dose constraint).

If the effective public dose of radon is lower than 0.4 mSv/a, the regulation reference radon concentration constraint can be calculated using Eq. (1). The regional radon background concentration is 28 Bq/m^3. The derived radon concentration constraint is 69.6 Bq/m^3 for a residence factor of 0.3 and 59.2 Bq/m^3 for a residence factor of 0.4.

The radiation protection distance can be determined according to the radon concentration contour map. As shown in Figure 10, the radiation protection range is set for the production conditions using the monitoring data on the left side. On the right side, the radiation protection distance range is set based on the simulated model estimation data. The blue line in Figure 10 is the proposed radiation protection distance for a residence factor of 0.4, and the red line is the proposed radiation protection distance for a residence factor of 0.3.

It can be seen that the radiation protection distance delimited according to the monitored radon concentration contour is significantly larger than that delimited according to the simulated data, and the edge is not neat. The radiation protection distance ranges from 400 m to 750 m around the ventilation shaft, and it is delimited according to the actual situation. Based on the simulated data, the radiation protection distance ranges from 300 m to 500 m.

In practice, if the relocation and active protection measures are cost efficient, a simple rectangular boundary can be used to frame the outer

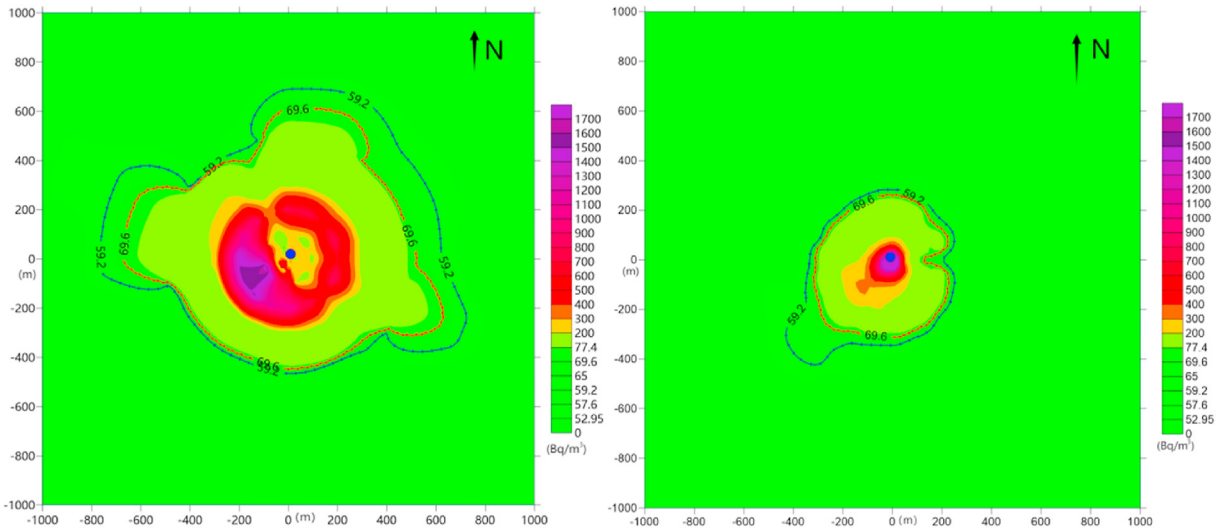

Figure 10. Comparison of the radiation protection distances based on the onsite measured data and simulated data.

boundary of the contour line and can be used as the radiation protection distance. This would make publicity and management easier. However, when relocation costs are high or relocation is difficult to implement, the radiation protection distance can be delimited according to the boundary of the contour line as closely as possible, and the key population groups can be included in the occupational radiation monitoring plan to strengthen services within a certain range outside the boundary.

With the development of UMM radiation protection technology and the improvement of the management level, the effective public dose can be further reduced, especially the liquid path and food path, and the public radiation dose can be constantly reduced. It can be assumed that the proportion of effective public radiation doses from radon channels would be higher and higher. This will increase the acceptable radon concentration constraint. Thus, the investment cost of radiation protection distance relocation and other activities will decrease.

For proposed new UMM facilities, it is necessary to determine the radiation protection distance through atmospheric model estimation due to the inability to measure the ambient radon concentration. Therefore, it is suggested that the recommended radiation protection distance be determined through analogy to existing facilities; the radiation protection distance should be adjusted in a timely manner after operations begin, and radon concentration measurements can be obtained in order to accurately set the radiation protection distance.

6. Conclusions

Systematic investigation of the radon concentration distribution regularities was carried out on a ventilation shaft of a typical underground UMM facility. Radon concentration monitoring was carried out for 1 year in 16 directions around the ventilation shaft and at eight points from 50 m to 1000 m from the shaft in each direction. The instantaneous radon, short-term cumulative radon, and long-term cumulative radon integrated monitoring methods were adopted to ensure the representativeness of the radon concentration monitoring data. The distribution characteristics of the radon concentration around the typical mine were obtained, and a dataset for the radon concentration around the ventilation shaft was formed.

The results of this study revealed the spatial and temporal characteristics and regularities of the radon concentration around the ventilation shaft. The relationship between the radon monitoring period and the data results was determined, confirming that the monitored radon concentrations were higher at night than during the day. It is recommended that short-term 24-h cumulative radon monitoring data be obtained in fine weather for proper UMM radon monitoring. This method of radon concentration monitoring is characterized by a good data representativeness and has the advantages of simultaneous large-batch sampling; so, it can further improve the timeliness of data collection. However, the research is base on a typical case study, more cases are require in subsequent studies.

In this study, the distribution patterns of the measured radon concentration and the atmospheric diffusion model estimates were compared. It was found that the simulated data underestimated the radon concentration in the upwind direction, and thus, it is necessary to be cautious when formulating a radiation protection strategy based on estimated data alone.

A method of delimiting the radiation protection distance was proposed. According to the radiation protection targets, different radiation protection distances can be optimized in different directions around the facility according to the radon distribution characteristics. In practice, the radiation protection distance can be estimated in advance through analogy to modeling of facilities, and the radiation protection distance can be adjusted according to the measured radon concentration distribution characteristics after operation of the UMM facility begins.

Declarations

Author contribution statement

Hui Zhang; Jie Gao; Yunlong Bai, Ph.D; Lei Zhou; Lechang Xu, Ph.D: Conceived and designed the experiments; Performed the experiments; Analyzed and interpreted the data; Contributed reagents, materials, analysis tools or data; Wrote the paper.

Funding statement

This research did not receive any specific grant from funding agencies in the public, commercial, or not-for-profit sectors.

Data availability statement

Data will be made available on request.

Declaration of interest's statement

The authors declare no competing interests.

Additional information

No additional information is available for this paper.

References

Brusin, J.H., 2007. Radiation protection. Radiol. Technol. 78, 378–392.

Chen, J., 2005. A review of radon doses. Radiat. Protect. Manag. 22, 27.

Davies, A., Britton, R., 2020. Improving the sensitivity and reliability of radionuclide measurements at remote international monitoring stations. J. Environ. Radioact. 216, 106187.

De Pree, T.A., 2020. The politics of baselining in the Grants uranium mining district of northwestern New Mexico. J. Environ. Manag. 268, 110601.

Dong, X., Zhuang, S., Fang, S., Li, H., Cao, J., 2021. Multi-scenario validation of CALMET-RIMPUFF for local-scale atmospheric dispersion modeling around a nuclear powerplant site with complex topography. J. Environ. Radioact. 229, 106547.

Durridge, 2011. RAD7 Radon Detector—User Manual. Durridge Company Inc. Bedford.

Elísio, S., Peralta, L., 2020. Development of a low-cost monitor for radon detection in air. Nucl. Instrum. Methods Phys. Res. Sect. A Accel. Spectrom. Detect. Assoc. Equip. 969, 164033.

Fijałkowska-Lichwa, L., 2014. Short-term radon activity concentration changes along the underground educational tourist route in the old uranium mine in Kletno (Sudety Mts., SW Poland). J. Environ. Radioact. 135, 25–35.

Gaskin, J., Coyle, D., Whyte, J., Birkett, N., Krewksi, D., 2019. A cost effectiveness analysis of interventions to reduce residential radon exposure in Canada. J. Environ. Manag. 247, 449–461.

Girault, F., Perrier, F., 2012. Measuring effective radium concentration with large numbers of samples. Part I–experimental method and uncertainties. J. Environ. Radioact. 113, 177–188.

Han, J.-h., Kim, Y., 2021. Comparative analysis of the CALPUFF and AERMOD atmospheric dispersion models for ready-mixed concrete manufacturing facilities generating particulate matter. J. Environ. Healt. Sci. 47, 267–278.

Kotrappa, P., Stieff, A., Stieff, F., 2013. Advanced calibration equations for E-PERM® electret ion chambers. In: Proceedings of the 2013 International Radon Symposium, pp. 10–19.

Kovalets, I.V., Asker, C., Khalchenkov, A.V., Persson, C., Lavrova, T.V., 2017. Atmospheric dispersion of radon around uranium mill tailings of the former Pridneprovsky Chemical Plant in Ukraine. J. Environ. Radioact. 172, 173–190.

Liu, F.-d., Pan, Z.-q., Liu, S.-l., Chen, L., Chen, L., Wang, C.-h., 2017. The estimation of the number of underground coal miners and normalization collective dose at present in China. Radiat. Protect. Dosim. 174, 302–307.

Loffredo, F., Scala, A., Serra, M., Quarto, M., 2021. Radon risk mapping: a new geostatistical method based on Lorenz Curve and Gini index. J. Environ. Radioact. 233, 106612.

Ma, J., Yi, H., Tang, X., Zhang, Y., Xiang, Y., Pu, L., 2013. Application of AERMOD on near future air quality simulation under the latest national emission control policy of China: a case study on an industrial city. J. Environ. Sci. 25, 1608–1617.

Marsh, J.W., Tomášek, L., Laurier, D., Harrison, J.D., 2021. Effective dose coefficients for radon and progeny: a review of icrp and unscear values. Radiat. Protect. Dosim. 195, 1–20.

Obodunrin, O., 2022. Location based approach to determining the effective dose from radon concentrations in residential environments. J. Appl. Sci. Environ. Manag. 26, 537–541.

Shweikani, R., Ka'aka, M., Bardan, R., 2014. ChargingE-perm for radon measurements. Radiat. Meas. 62, 10–14.

Unger, C.J., Everingham, J.-A., Bond, C.J., 2020. Transition or transformation: shifting priorities and stakeholders in Australian mined land rehabilitation and closure. Australas. J. Environ. Manag. 27, 84–113.

Vandenhove, H., Sweeck, L., Mallants, D., Vanmarcke, H., Aitkulov, A., Sadyrov, O., Savosin, M., Tolongutov, B., Mirzachev, M., Clerc, J., 2006. Assessment of radiation exposure in the uranium mining and milling area of Mailuu Suu, Kyrgyzstan. J. Environ. Radioact. 88, 118–139.

Xie, D., Wang, H., Kearfott, K.J., Liu, Z., Mo, S., 2014. Radon dispersion modeling and dose assessment for uranium mine ventilation shaft exhausts under neutral atmospheric stability. J. Environ. Radioact. 129, 57–62.

Yarmoshenko, I., Zhukovsky, M., Onishchenko, A., Vasilyev, A., Malinovsky, G., 2021. Factors influencing temporal variations of radon concentration in high-rise buildings. J. Environ. Radioact. 232, 106575.

Zhou, Q., Liu, S., Xu, L., Zhang, H., Xiao, D., Deng, J., Pan, Z., 2019. Estimation of radon release rate for an underground uranium mine ventilation shaft in China and radon distribution characteristics. J. Environ. Radioact. 198, 18–26.